Structural phase transitions of phosphorene induced by applied strains

Ting Hu and Jinming Dong*

Group of Computational Condensed Matter Physics, Department of Physics, National Laboratory of Solid State Microstructures, Nanjing University, Nanjing 210093, People's Republic of China

(Received 29 April 2015; revised manuscript received 1 August 2015; published 25 August 2015)

The effects of normal compressive strain and in-plane strain on the structures of phosphorene have been investigated by using first-principles calculations. It is quite intriguing to find that a structural transformation from pristine Z-phosphorene to a new A-phosphorene occurs under the normal compressive strain of $\varepsilon = 48\%$ or the anisotropic biaxial in-plane strain of $\varepsilon_x = -16\%$ and $\varepsilon_y = 54\%$. In the extreme case where the pucker structure is flattened into a plane, the phosphorene structure is quite unstable at finite temperatures, transforming into another new H-phosphorene phase. The anisotropic structure of A-phosphorene gives rise to its direction-dependent mechanical properties whereas H-phosphorene exhibits isotropic mechanical properties. Both A-phosphorene and H-phosphorene are semiconductors with indirect band gaps of about 0.42 and 1.94 eV that use the Perdew-Burke-Ernzerhof exchange-correlation functional, respectively. The electronic properties of the two new phases are found to be sensitive to the magnitude and direction of the applied strains, which offer an effective method to modulate them in future device engineering.

DOI: 10.1103/PhysRevB.92.064114 PACS number(s): 68.35.Rh, 68.35.Gy, 73.22.−f, 61.46.−w

I. INTRODUCTION

Two-dimensional (2D) materials, such as graphene [1,2], silicene [3], and hexagonal-layered boron nitride [4] have been one of the most interesting subjects in condensed-matter physics for their distinctive electronic structures and promising applications in nanoelectronics and spintronics. Most recently, another 2D nanomaterial, i.e., the few-layer black phosphorus (phosphorene), has been successfully fabricated through mechanically cleaving bulk black phosphorus and immediately attracted considerable attention [5–8] in which the individual atomic layers are stacked together by van der Waals interactions.

Unlike the zero-gap semimetal graphene, the phosphorene exhibits a direct band gap, which can be modified from 1.51 eV of a monolayer to 0.59 eV of a five-layer sample [9]. Moreover, it is reported that the phosphorene has a high carrier mobility up to $1000\,\mathrm{cm^2\,V^{-1}\,s^{-1}}$ [5] and the phosphorene transistors achieved an appreciably high on/off ratio up to 10^4 at room temperature [6], making this material of great interest for future nanoelectronic applications. Furthermore, phosphorene has a characteristic puckered structure, leading to a substantial anisotropy of its mechanical behavior, electric conductance, and optical responses [6,10–12], which distinguishes it from many other isotropic 2D crystals.

The controlled introduction of strain into semiconductors is known to be an effective method to tune their microstructures and electronic properties. Recent work has demonstrated that the monolayer phosphorene exhibits a superior mechanical flexibility, which can hold a critical strain up to 30% [13]. It has been shown theoretically that phosphorene's electronic properties could be changed by an applied in-plane strain, inducing a direct-indirect band-gap transition as well as a semiconductor-metal transition [14,15]. The electronic band structure of phosphorene also undergoes a semiconductor-semimetal-metal transition under the normal compressive strain [16]. Moreover, a unique anisotropic conductance is observed in phosphorene, which can be controlled and even rotated by 90° under an appropriate uniaxial or biaxial strain [12].

In this paper, we have investigated the effect of a normal compressive strain and an in-plane strain on the geometric structures and electronic properties of phosphorene by using first-principles calculations. It is quite intriguing to find that by controlled introduction of mechanical deformation, structural phase transitions have been induced in phosphorene, producing two new phases with different mechanical and electronic properties from the pristine phosphorene, which are sensitive to the magnitude and direction of the applied strains.

The remainder of this paper is organized as follows. In Sec. II, the geometric structures and computational details are described. In Sec. III, the main numerical results and some discussions are given. Finally, in Sec. IV, a conclusion is presented.

II. MODEL AND METHOD

Unlike the plane structure of graphene, phosphorene has a characteristic puckered honeycomb lattice, buckling alternately by the zigzag lines. Each phosphorus atom is covalently bonded with three neighboring atoms within a rectangular unit cell, and there are four P atoms in one basic unit cell. The x and y axes are taken to be along the armchair and zigzag directions of phosphorene, respectively.

All calculations in this paper were performed by density functional theory in the generalized gradient approximation, implemented by the VASP code [17,18] in which the Perdew-Burke-Ernzerhof [19] exchange-correlation functional and the projector augmented-wave formalism [20] are employed. The layered structures are placed on the xy plane, and a large vacuum region is added in the z direction, making the closest distance between two adjacent nanosheets be 15 Å.

The geometric structure optimization was performed using the conjugated-gradient minimization scheme until the maximum residual force on each atom was less than

*Corresponding author: jdong@nju.edu.cn

 ©2015 American Physical Society

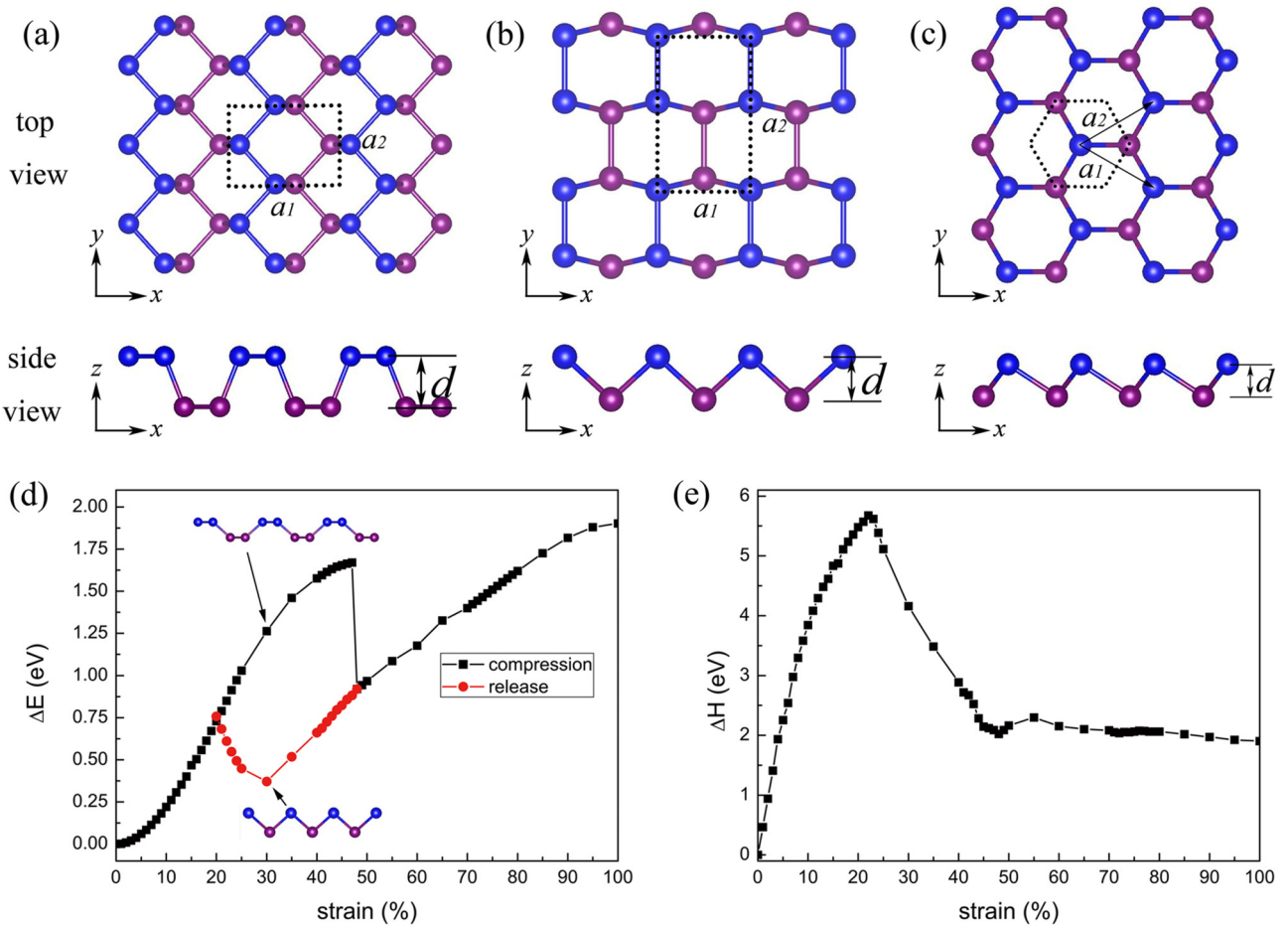

FIG. 1. (Color online) The optimized geometric structures of (a) pristine phosphorene, (b) A-phosphorene, and (c) H-phosphorene. The $a_1 \times a_2$ unit cell of pristine phosphorene is outlined by black dashed lines. Here, the P atoms in the upper (lower) half-layer are denoted by blue (purple) in order to clearly identify them in two different half-layers of the phosphorene. (d) The energy difference between strained and pristine phosphorene (ΔE) varying with normal compression. The black dots denote the compression process whereas the red dots represent the process of releasing the strain. (e) The relative enthalpy ΔH referring to the H_0 of pristine phosphorene as a function of strain in the compression process.

10^{-4} eV/Å. A plane-wave cutoff of 350 eV for phosphorene was used in our numerical calculations, and the energies were converged to 10^{-5} eV/atom. The reciprocal space of the supercell is sampled with a $30 \times 30 \times 1$ Monkhorst-Pack grid.

The optimized geometric structure of pristine phosphorene is presented in Fig. 1(a), which has a puckered honeycomblike lattice structure with its pucker height d of about 2.104 Å. The relaxed lattice constants of the monolayer phosphorene are $a_1 = 4.619$ and $a_2 = 3.298$ Å.

III. RESULTS AND DISCUSSIONS

A. Phase transitions of phosphorene under mechanical deformation

Starting from the relaxed phosphorene structure, a normal compressive strain was applied by varying the pucker height d. At each fixed height d, a constrained relaxation scheme was performed for optimizing the geometric structures in which the unit cell and atomic positions in the two half-layers of phosphorene were relaxed under a constraint of fixing the z coordinates of all atoms at each fixed height d. The applied strain was defined as $\varepsilon = \frac{d_0 - d}{d_0}$, where d_0 and d are the equilibrium and instantaneous pucker height, respectively.

It is found that the lattice parameter along the armchair direction increases significantly whereas that along the zigzag direction decreases slightly under the compression strains in the range from 1% to 47%. The electron localization function (ELF) analysis gives the ELF values larger than 0.5 between two P atoms, indicating that the geometric structure retains its original bonding configuration. However, as the compressive normal strain increased up to 48%, the continuous expansion of a_1 would break the P-P bonds, leading to a structural transformation of phosphorene with shrinkage of its lattice parameter along the armchair direction and expansion of that along the zigzag direction. Meanwhile, the P-P bond in the same half-layer turns to align along the y direction, and the P-P bond connecting the top and bottom half-layers deviates from the x direction, inducing a new geometrical phase of phosphorene.

The ground state of this new phase is then obtained by fully relaxing both the unit cell and the atomic positions without constraint, whose optimized geometric structure is shown in

Fig. 1(b). Unlike the puckered structure alternated by the zigzag lines in the pristine phosphorene, the new geometrical phase of phosphorene has a puckered structure alternated by the armchair lines, which thus can be called A-phosphorene, in contrast to the original phosphorus, called Z-phosphorene. The relaxed lattice constants of A-phosphorene are $a_1 = 3.268$ and $a_2 = 5.419$ Å, whereas its pucker distance is only $d = 1.493$ Å, being about 70% of that of Z-phosphorene.

The detailed analysis of the energy difference (ΔE) between the strained A-phosphorene and the pristine Z one, varying with normal compression, is presented in Fig. 1(d), from which it can be found that the energy difference ΔE increases monotonously with the strain in the range from 0% to 47%. However, when the normal strain increases over 47%, the ΔE experiences a sharp decrease by about 0.75 eV, indicating that the system transforms into a more stable phase. Further increase in the compressive strain makes the ΔE again increase monotonously.

To further confirm the phase transition at $\varepsilon = 48\%$, we used the A-phosphorene structure under $\varepsilon = 48\%$ as an initial configuration and then gradually release the strain. It is found that the system still remains in the A-phosphorene phase with the corresponding energy-strain relations, given by the red dots in Fig. 1(d). The energy first lowers down as the strain releases from 48% to about 30% at which the ΔE value reaches a minimum. And then it increases with a further increase in the pucker height. When the strain reduces to $\varepsilon = 20\%$, the energy of A-phosphorene becomes larger than that of Z-phosphorene.

We have also calculated the enthalpy of the system, which is defined as $H = E + pV = E + \frac{\partial E}{\partial d} d$, where E and d are the energy and pucker height of strained phosphorene. The relative enthalpy ΔH referring to the H_0 of pristine phosphorene as a function of compressive strain is plotted in Fig. 1(e) from which we can find a minimum of enthalpy at $\varepsilon = 48\%$. Phosphorene with a strain over 47% also holds very low enthalpy, indicating that the A-phosphorene is a stable structure under high pressure.

It is also interesting to find that the pucker structure of Z-phosphorene could be compressed into a flat hexagonal plane structure (i.e., $\varepsilon = 100\%$) under a very high pressure but is quite unstable at finite temperatures. The first-principles finite temperature molecular dynamics (MD) simulations found that even at a very low temperature of 2 K, the wrinkle in the z-axis direction would appear in the flat plane structure, leading to a structural reconstruction, which finally induces a new puckered phosphorene phase (H-phosphorene), as seen in the Supplemental Material [21].

The optimized geometric structure of the new H-phosphorene is shown in Fig. 1(c), which has a hexagonal Wigner-Seitz cell, containing only two atoms. The lattice constant of H-phosphorene is $a_1 = a_2 = 3.277$ Å, and the pucker distance is $d = 1.238$ Å. It can be found that the H-phosphorene phase structure is different from both A-phosphorene and Z-phosphorene with an anisotropic ridge structure but transforms into an isotropic puckered one, which is the same as the puckered silicene, where the A and B sublattices sit on two vertically separated planes.

In order to investigate the stabilities of different phases, we have calculated their binding energies $E_b = E - NE_P$, where E and E_P are the energies of phosphorene and the isolated phosphorus atom, respectively, and N is the number of phosphorus atoms in phosphorene. Our results for the binding energies as well as the optimum geometric parameters of different phases are summarized in Table I. It is found that the binding energy of H-phosphorene is only about 1 meV/atom higher than that of Z-phosphorene, suggesting H-phosphorene is almost equivalently stable to Z-phosphorene. A-phosphorene has higher binding energy than that of the most stable Z-phosphorene by 92 meV/atom.

TABLE I. The calculated geometric parameters and binding energies of different phosphorene phases are summarized.

	a_1 (Å)	a_2 (Å)	d (Å)	E_b (eV/atom)
Z-phosphorene	4.619	3.298	2.104	−3.477
A-phosphorene	3.268	5.419	1.493	−3.385
H-phosphorene	3.277	3.277	1.238	−3.476

In addition, the first-principles finite temperature MD simulations are further performed to confirm the stabilities of A-phosphorene and H-phosphorene, finding that both of them are stable at room temperatures and even 500 K in our simulation time of 10 ps.

The phonon spectra of different phases have also been calculated, and no imaginary phonon modes are found in H-phosphorene, further confirming the dynamic stability of the new phase. However, A-phosphorene with higher energy is found to show imaginary phonon modes along Γ-X in its phonon spectrum, calculated in different supercell sizes of it. That most probably means there might exist some possible reconstructions along the x direction in its supercells, which is worth investigating in future work.

It is also noticed that the normal-compression-induced A- and H-phosphorenes had been postulated as γ-P and β-P, respectively, by previous theoretical work as possible phosphorus allotropes [22].

It is found that the large structural deformations in monolayer phosphorene can also be induced by tensile strains in addition to the high normal pressure. In practice, the monolayer nanomaterial can be put on a flexible substrate, realizing the independent control of its lattice parameters of a_1 and a_2. We have also investigated the geometric structures of phosphorene under in-plane strain. It is interesting to find that the in-plain strain could also induce the structural transformation in phosphorene. For example, when Z-phosphorene is subject to a biaxial in-plain strain, composed of a compressive ε_x along the armchair direction but a tensile ε_y along the zigzag direction, increasing gradually to $\varepsilon_x = -16\%$ and $\varepsilon_y = 54\%$, the structure would also turn into the A-phosphorene phase. Besides, when the anisotropic strain $\varepsilon_x = 12\%$ and $\varepsilon_y = 35\%$, or the isotropic strain of 29% is applied, the pristine Z-phosphorene will evolve into the flat hexagonal structure, which is quite unstable at finite temperatures and will quickly transform into H-phosphorene at a very low temperature.

B. Mechanical properties of different phosphorene phases

The controlled strain is an effective method in device engineering. And the fundamental studies on the mechanical properties of these new phosphorene phases are crucial to

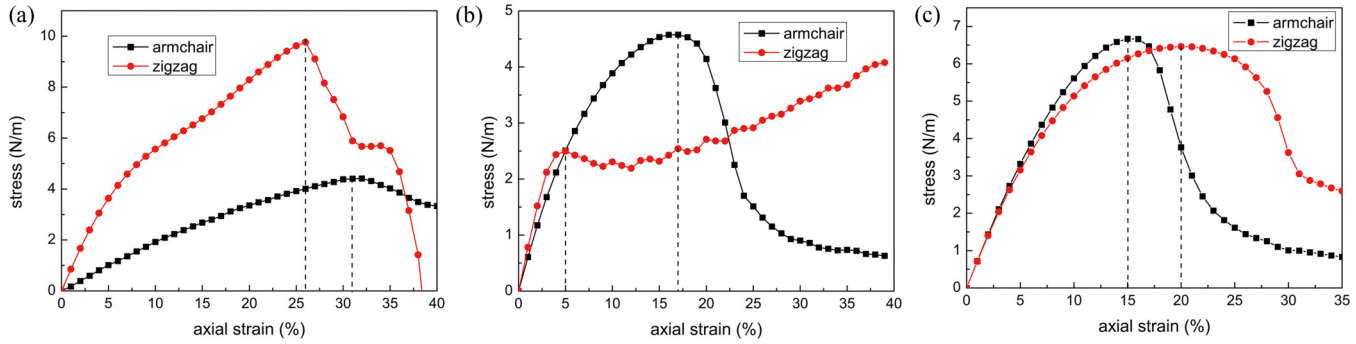

FIG. 2. (Color online) The stress-strain relation for (a) Z-phosphorene, (b) A-phosphorene, and (c) H-phosphorene.

know how they can possibly be used in the high performance electromechanical devices. It has already been reported by previous studies that Z-phosphorene possesses supermechanical flexibility and can withstand a tensile strain up to 30%. Young's modulus was also found to depend sensitively on the direction due to its extraordinary anisotropic puckered structure [13]. Starting from the fully relaxed structures of A- and H-phosphorenes, an in-plane uniaxial tensile strain is applied along either the armchair or the zigzag direction to explore their mechanical properties.

The material strength is the ultimate stress required to break a perfect crystal. To estimate the strengths of A- and H-phosphorenes, we have calculated the stress as a function of applied strain using the method described in the Refs. [23,24]. By analogy with the study in Z-phosphorene [14], the stress in the 2D monolayers is modified to be the force per unit length.

The calculated stress-strain relations of A- and H-phosphorenes are depicted in Figs. 2(b) and 2(c), respectively, whereas the result of Z-phosphorene is also given in Fig. 2(a) as a comparison. It shows that the ideal strengths of Z-phosphorene are 4.41 and 9.76 N/m, corresponding to the critical strains of 32% and 26% in the armchair and zigzag directions, respectively, which are in good agreement with previous studies [13,14]. The elastic regime of three phases can be inferred from the stress-strain curve, which are all approximately linear in the strain ranges of 3% to 4% in which we say that phosphorenes are in the elastic regime.

Similar to Z-phosphorene, the anisotropic structure of A-phosphorene also gives rise to its direction-dependent mechanical properties. From the stress-strain relation in Fig. 2(b), it can be found that A-phosphorene can sustain a stress up 4.58 N/m in the armchair direction at the corresponding critical strain of 17%. Whereas for the tensile strain loaded in the zigzag direction, a yielding point appears at 5% tensile strain. After that, a further increase in the strain would not break the geometric structure of A-phosphorene but only stretch its pucker structure along the zigzag direction. A-phosphorene retains its bonding configuration even under a tensile strain up to 40% applied in the zigzag direction.

For H-phosphorene, the mechanical behaviors are isotropic in the elastic regime as shown in Fig. 2(c). The ideal strengths are 6.67 and 6.46 N/m in the armchair and zigzag directions, corresponding to the critical strains of 15% and 20%, respectively.

In addition to the ideal tensile strength and critical strain, we further calculated in-plane elastic stiffness constants, effective Young's/shear moduli, as well as Poisson's ratios to assess the mechanical response of different phosphorene phases.

For the two-dimensional structures, the in-plane stress-strain relation can be written as [25]

$$\begin{bmatrix}\sigma_x\\ \sigma_y\\ \tau_{xy}\end{bmatrix} = \frac{1}{1-\nu_{xy}\nu_{yx}}\begin{bmatrix}E_x & \nu_{yx}E_x & 0\\ \nu_{xy}E_y & E_y & 0\\ 0 & 0 & G_{xy}(1-\nu_{xy}\nu_{yx})\end{bmatrix} \times \begin{bmatrix}\varepsilon_x\\ \varepsilon_y\\ \gamma_{xy}\end{bmatrix} = \begin{bmatrix}C_{11} & C_{12} & 0\\ C_{21} & C_{22} & 0\\ 0 & 0 & C_{66}\end{bmatrix}\begin{bmatrix}\varepsilon_x\\ \varepsilon_y\\ \gamma_{xy}\end{bmatrix},$$

where $\nu_{ij} = -\frac{d\varepsilon_j}{d\varepsilon_i}$ is the Poisson ratio with tensile strain applied in the direction i and the response strain in the direction j, E_i is Young's modulus along the ith axis, G_{xy} is the shear modulus on the xy plane, and γ_{xy} is the shear strain on the xy plane. Since the thickness for monolayer phosphorene is not considered, the unit for the stress as well as the elastic moduli is force per unit length (N/m) rather than force per unit area (N/m^2 or Pa).

In order to figure out the above constants, we have scanned the energy surface of the three phases in their elastic regimes: $-3\% < \varepsilon_x < 3\%$, $-3\% < \varepsilon_y < 3\%$, and $-2\% < \gamma_{xy} < 2\%$ in a step of 0.5%. The strain-energy relation is then obtained $E_S = a_1\varepsilon_x^2 + a_2\varepsilon_y^2 + a_3\varepsilon_x\varepsilon_y + a_4\gamma_{xy}^2$ by parabolic fitting of the strain-energy surface, where the coefficients a_i are fitted parameters. We then calculated the in-plane elastic stiffness constant C_{ij}, which is defined as $C_{ij} = \frac{1}{A_0}\frac{\partial E_S^2}{\partial\varepsilon_i\partial\varepsilon_j}$, where A_0 is the equilibrium area of different phosphorene phases. Consequently, Young's/shear moduli and Poisson's ratio can be derived as follows:

$$E_x = \frac{1}{A_0}\left(2a_1 - \frac{a_3^2}{2a_2}\right), \quad E_y = \frac{1}{A_0}\left(2a_2 - \frac{a_3^2}{2a_1}\right),$$
$$G_{xy} = \frac{2a_4}{A_0}, \quad \nu_{xy} = \frac{a_3}{2a_2}, \quad \nu_{yx} = \frac{a_3}{2a_1}.$$

The calculated Young's/shear moduli and Poisson's ratios for different phases are listed in Table II. The values of Z-phosphorene are consistent with previous studies [13,26]. Due to the anisotropic property of A-phosphorene, Young's modulus and Poisson's ratios also have different values in the

TABLE II. The calculated Young's/shear moduli and Poisson's ratios for different phases of phosphorene.

	Young's modulus (N/m)			Poisson's ratio	
Structure	Armchair	Zigzag	Shear modulus (N/m)	Armchair	Zigzag
Z-phosphorene	22.15	92.01	22.31	0.71	0.17
A-phosphorene	68.28	85.65	19.84	−0.029	−0.023
H-phosphorene	77.64	77.64	35.23	0.11	0.11

armchair and zigzag directions. Young's modulus in the zigzag direction is about 1.25 times larger than its counterparts in the armchair direction, exhibiting much less anisotropy compared with Z-phosphorene. Whereas for H-phosphorene, the values of Young's modulus or Poisson's ratios in different directions are equal, indicating the isotropic character of Z-phosphorene.

It is worth pointing out that A-phosphorene exhibits a negative Poisson's ratio under uniaxial strains along both armchair and zigzag directions in the elastic regime. With a further increase in the tensile strain over 3%, the Poisson ratios turn into positive values.

C. Variation in electronic properties with applied strain in different phosphorene phases

The electronic properties of undeformed A- and H-phosphorenes have been calculated, and their band structures are presented in Figs. 3(a) and 3(c), respectively, denoted by black lines. A-phosphorene is a semiconductor with an indirect band gap of about 0.42 eV. Its conduction-band minimum (CBM) and valence-band maximum (VBM) are located on the points between Γ-*X*. H-phosphorene is also an indirect-band-gap semiconductor with its CBM at a point between Γ-*X* and its VBM at a point between Γ-*Y*. The band gap of H-phosphorene is about 1.94 eV.

To assess the effect of strain modulation on electronic properties, the band structures of A- and H-phosphorenes under both isotropic and uniaxial strains along the armchair or zigzag directions have been studied. Figure 3(a) compares the electronic band structures of undeformed and deformed A-phosphorene. The tensile strain along the armchair (*y*) direction raises the CBM between Γ-*X* whereas the energy of the VBM decreases with the increasing strain, leading to an increase in the band gap. On the other hand, when A-phosphorene is subjected to compressive strain along the armchair direction, whose band structure is not shown here,

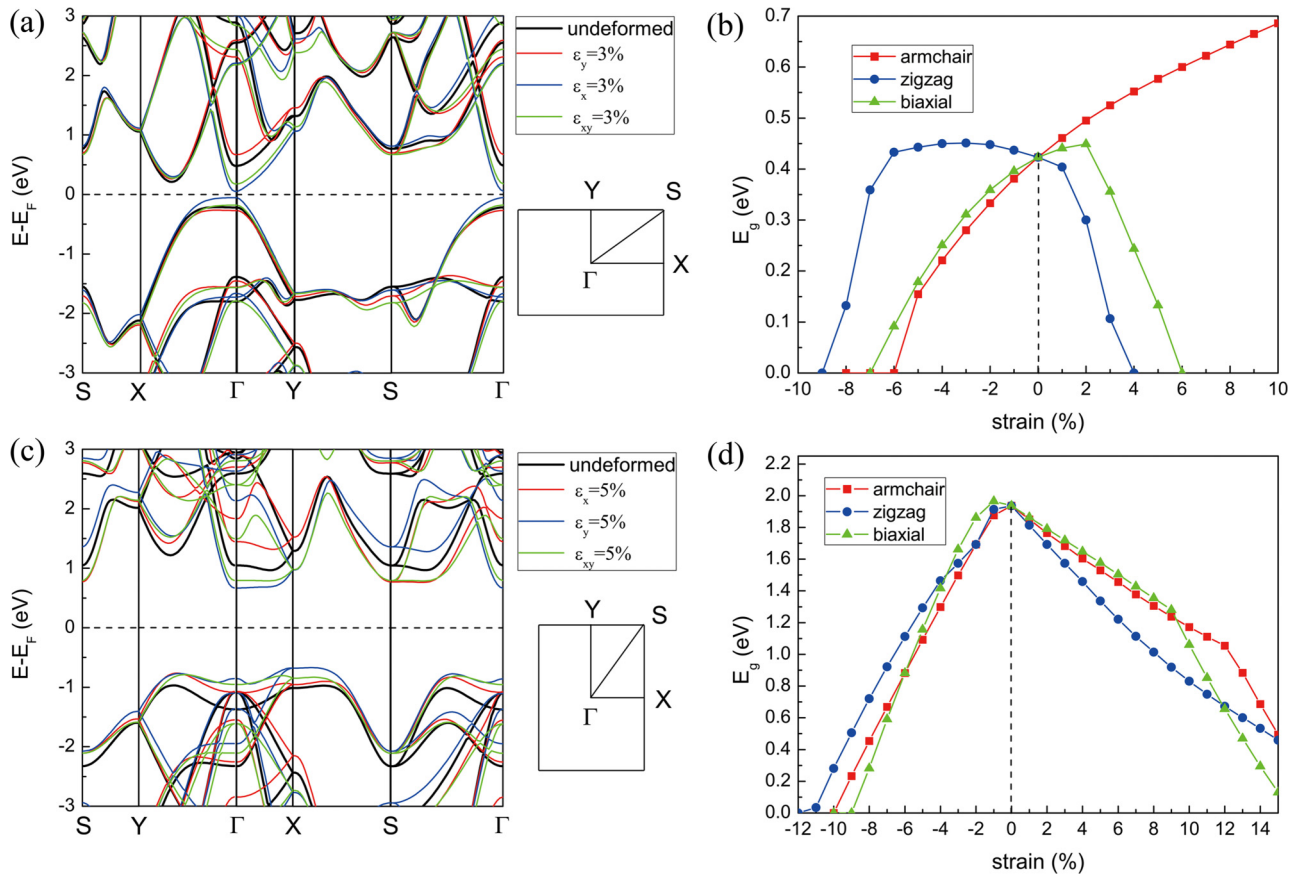

FIG. 3. (Color online) The band structures of (a) A-phosphorene and (c) H-phosphorene under different kinds of strains. The corresponding band-gap variations in A- and H-phosphorenes under different kinds of strains are shown in (b) and (c), respectively.

both the CBM and the VBM move close to the Fermi level, thereby reducing its band gap quickly.

When the uniaxial tensile strain is taken along the zigzag (x) direction, the state on the conduction band located at the Γ point moves down and becomes a new CBM at a strain of about 2%. At the same time, the dispersion relation of the highest valence band will gradually change, which makes the pristine VBM point, lying between the Γ-X, move to another point at Γ, inducing so an indirect-direct band-gap transition at $\varepsilon_x = 2\%$. The isotropic strain effect on the electronic structures of A-phosphorene is also studied, which exhibit a similar transition from an indirect band gap to a direct band gap under a tensile strain of about 3%.

The energy gap variation in A-phosphorene with different uniaxial strains is shown in Fig. 3(b) where the negative value of the strain denotes the compressive strain. It can be seen that the band gap increases monotonously with the strain applied along the armchair direction, and a semiconductor-metal transition happens at a compressive strain of about −6%. When the strain is applied along the zigzag direction, the band gap decreases rapidly with the tensile strain, making the system turn into a metal at $\varepsilon_x = 4\%$. However, under the compressive strain, the band gap slightly increases from 0.42 to 0.45 eV as the strain increases to $\varepsilon_x = -3\%$. And a further increase in the compressive strain up to about $\varepsilon_x = -6\%$ will slightly decrease the gap to about 0.43 eV and then quickly reduce the band gap to zero at $\varepsilon_x = -9\%$. When the biaxial isotropic strain is applied, the compressive strain gives rise to a monotonous reduction of the band gap to zero at $\varepsilon_{xy} = -7\%$, whereas the tensile strain can initially increase the band gap to its maximum value of 0.45 eV at $\varepsilon_{xy} = 2\%$ and then reduce it to zero at $\varepsilon_{xy} = 6\%$.

Similarly, the electronic structures of H-phosphorene under different strains are presented in Fig. 3(c), and the corresponding band-gap variations are depicted in Fig. 3(d). It can be found that both the compressive and the tensile uniaxial strains will reduce its band gap, except for the biaxial compressive strain at $\varepsilon_{xy} = -1\%$, which increases the band gap by 0.03 eV. Increasing further the compressive strain leads to the band-gap reduction until the gap closure, which occurs at $\varepsilon_x = -10\%$, $\varepsilon_y = -12\%$, and $\varepsilon_{xy} = -9\%$. While under the external tensile strain, no semiconductor-metal transition has been observed in our strain range to 15%.

IV. CONCLUSIONS

The effects of normal compressive strain and in-plane strains on the structures of phosphorene have been investigated by using first-principles calculations. It is quite intriguing to find that by controlled introduction of mechanical deformation, a structural transformation from pristine Z-phosphorene to a new A-phosphorene can occur under either a normal compressive strain of $\varepsilon = 48\%$ or an anisotropic biaxial strain of $\varepsilon_x = -16\%$ and $\varepsilon_y = 54\%$. On the other hand, the flat plane phosphorene structure obtained under a high normal pressure is found to be unstable at finite temperatures, which is easily transformed into a new H-phosphorene phase. The mechanical and electronic properties of the two new phosphorene phases are also studied by first-principles calculations. The anisotropic structure of A-phosphorene gives rise to its direction-dependent mechanical properties with Young's modulus in the zigzag direction about 1.25 times larger than their counterparts in the armchair direction. H-phosphorene exhibits isotropic mechanical properties with its effective Young's modulus to be 77.64 N/m. Both A-phosphorene and H-phosphorene are semiconductors with indirect band gaps of about 0.42 and 1.94 eV, respectively. The electronic properties of the two new phases are found to be sensitive to the magnitude and direction of the applied strains, which offers an effective method to modulate them in device engineering.

ACKNOWLEDGMENTS

This work was supported by the State Key Program for Basic Research of China through Grant No. 2011CB922100Q. Our numerical calculations were performed at the High Performance Computing Center of Nanjing University.

[1] K. Novoselov, A. Geim, S. Morozov, D. Jiang, Y. Zhang, S. Dubonos, I. Grigorieva, and A. Firsov, Science **306**, 666 (2004).
[2] Y. Zhang, Y. Tan, H. Stormer, and P. Kim, Nature (London) **438**, 201 (2005).
[3] S. Cahangirov, M. Topsakal, E. Akturk, H. Sahin, and S. Ciraci, Phys. Rev. Lett. **102**, 236804 (2009).
[4] M. Topsakal, E. Akturk, and S. Ciraci, Phys. Rev. B **79**, 115442 (2009).
[5] L. Li, Y. Yu, G.-J. Ye, Q. Ge, X. Ou, H. Wu, D. Feng, X.-H. Chen, and Y. Zhang, Nat. Nanotechnol. **9**, 372 (2014).
[6] H. Liu, A. T. Neal, Z. Zhu, D. Tomanek, and P. D. Ye, ACS Nano **8**, 4033 (2014).
[7] F. Xia, H. Wang, and Y. Jia, Nat. Commun. **5**, 4458 (2014).
[8] E. S. Reich, Nature (London) **506**, 19 (2014).
[9] J. Qiao, X. Kong, Z.-X. Hu, F. Yang, and W. Ji, Nat. Commun. **5**, 4475 (2014).
[10] V. Tran, R. Soklaski, Y. Liang, and L. Yang, Phys. Rev. B **89**, 235319 (2014).
[11] J.-W. Jiang and H. S. Park, Nat. Commun. **5**, 4727 (2014).
[12] R. Fei and L. Yang, Nano Lett. **14**, 2884 (2014).
[13] Q. Wei and X. Peng, Appl. Phys. Lett. **104**, 251915 (2014).
[14] X. Peng, Q. Wei, and A. Copple, Phys. Rev. B **90**, 085402 (2014).
[15] T. Hu, Y. Han, and J. Dong, Nanotechnology **25**, 455703 (2014).
[16] A. S. Rodin, A. Carvalho, and A. H. Castro Neto, Phys. Rev. Lett. **112**, 176801 (2014).
[17] G. Kresse and J. Hafner, Phys. Rev. B **48**, 13115 (1993).
[18] G. Kresse and J. Furthmüller, Comput. Mater. Sci. **6**, 15 (1996).
[19] J. P. Perdew, K. Burke, and M. Ernzerhof, Phys. Rev. Lett. **77**, 3865 (1996).
[20] G. Kresse and D. Joubert, Phys. Rev. B **59**, 1758 (1999).

[21] See Supplemental Material at http://link.aps.org/supplemental/10.1103/PhysRevB.92.064114 for videos of the first-principles finite temperature MD simulations, showing the transition from flat phosphorene to H-phosphorene at 10 K.
[22] J. Guan, Z. Zhu, and D. Tománek, Phys. Rev. Lett. **113**, 046804 (2014).
[23] D. Roundy and M. L. Cohen, Phys. Rev. B **64**, 212103 (2001).
[24] W. Luo, D. Roundy, M. L. Cohen, and J. W. Morris, Phys. Rev. B **66**, 094110 (2002).
[25] J. Zhou and R. Huang, J. Mech. Phys. Solids **56**, 1609 (2008).
[26] M. Elahi, K. Khaliji, S. M. Tabatabaei, M. Pourfath, and R. Asgari, Phys. Rev. B **91**, 115412 (2015).